Range Error Detection Caused by Occlusion in Non-Coaxial LADARs for Scene Interpretation

Bingbing Liu,
Martin Adams, and Wijerupage Sardha Wijesoma
School of Electrical & Electronics Engineering, Nanyang Technological University, Singapore

Javier Ibañez-Guzmán
Renault, Research Division, Electronics Systems Department, ■, France

Received 19 July 2004; accepted 19 May 2005

When processing laser detection and ranging (LADAR) sensor data for scene interpretation, for example, for the purposes of feature extraction and/or data association in mobile robotics, most previous work models such devices as processing range data which follows a normal distribution. In this paper, it is demonstrated that commonly used LADARs suffer from incorrect range readings at changes in surface reflectivity and/or range discontinuities, which can have a much more detrimental effect on such algorithms than random noise. Most LADARs fall into two categories: coaxial and separated transmitter and receiver configurations. The latter offer the advantage that optical crosstalk is eliminated, since it can be guaranteed that all of the transmitted light leaves the LADAR and is not in any way partially reflected within it due to the beam-splitting techniques necessary in coaxial LADARs. However, they can introduce a significant disparity effect, as the reflected laser energy from the target can be partially occluded from the receiver. As well as demonstrating that false range values can result due to this occlusion effect from scanned LADARs, the main contribution of this paper is that the occurrence of these values can be reliably predicted by monitoring the received signal strength and a quantity we refer to as the "transceiver separation angle" of the rotating mirror. This paper will demonstrate that a correct understanding of such systematic errors is essential for the correct further processing of the data. A useful design criterion for the optical separation of the receiver and transmitter is also derived for noncoaxial LADARs, based on the minimum detectable signal amplitude of a LADAR and environmental edge constraints. By investigating the effects of various sensor and environmental parameters on occlusion, some advice is given on how to make use of noncoaxial LADARs correctly so as to avoid range errors when scanning environmental discontinuities. © 2005 Wiley Periodicals, Inc.

Journal of Robotic Systems 22(10), 1–XXXX (2005) © 2005 Wiley Periodicals, Inc.
Published online in Wiley InterScience (www.interscience.wiley.com). • DOI: XXXX

1. INTRODUCTION

The work in this paper is inspired by the processing of LADAR range data for the detection of features or interpretation of data for mobile robot navigation.[1–3] In mobile robotics, range sensing is often a crucial component of navigational and localization tasks.[4–7] Laser detection and ranging sensors, or LADARs, with range and bearing information, have become an integral component of many simultaneous localization and map building systems, due to their accuracy and relatively low cost. Feature detection algorithms are often based on probabilistic methods which attempt to extract information from the range data in an optimal manner, on the assumption that the range data is corrupted with Gaussian noise. For example Guivant *et al.* have made an observation model for their Kalman filter based outdoor navigation system, assuming Gaussian noise.[5] Arras formulated the detection of line segments in Hough space and was able to generate line segment estimates and their associated covariances, based on the simple model that each LADAR range value was accompanied by assumed known, Gaussian noise.[8] Adams was able to detect range/reflectance discontinuities, by optimally weighting new range data with simple recursive line and constant curvature models—again based on range data Gaussian noise assumptions.[1,9]

In the experience of the authors, such feature extraction algorithms often fail due to other systematic, unmodeled errors from LADARs. While it is acknowledged that an estimate of range variance has a large effect on, for example, Kalman Filter based and scale space detection algorithms,[3,10] such methods can fail catastrophically when range errors due to *cross-talk*,[11] *disparity*,[12] or *multi-path effects*[1] occur. Removing such "outliers" from range data can be achieved with limited success with standard techniques such as median filters, based on certain assumptions about the erroneous range data.[13] It is argued here, however, that range errors should, and can, be estimated and eliminated or replaced, based on the physics of the LADAR and its scanning technique.

This paper will demonstrate that, besides the cross-talk and multipath effects (sometimes referred to as mixed pixels.[11]) that have been documented in the literature,[11,14–16] significant range errors can also occur due to disparity caused by a combination of transmitter and receiver separation and the scanning reflection principle, to the authors' knowledge, an effect previously not examined in the literature for LADARs.

First, an introduction to the 3D scanning LADAR systems used in this work will be presented in Section 2. Then, in Section 3 an overview of the range errors of LADARs due to different causes, namely occlusion, cross-talk and random noise, will be presented. It will be shown that significant range errors occur at, or near, range discontinuities. Such range errors have a detrimental effect on feature detection algorithms which attempt to isolate such range/intensity changes and then use such "end" range points for future data association.[17,18] The physical cause of this effect will be studied in detail in Section 4 and a theoretical model will be derived which allows such errors to be predicted, detected and removed from range scans. In particular it will be shown that the amplitude of the received signal will follow well defined profiles as the scanning mirror rotates, which depends on the orientation of the scanning mirror relative to the LADAR's transmitting and reception apertures.

It is noticed that unlike the mixed pixels and cross-talk effects noted in the previous literature, this effect is actually *independent* of the range detection method [time-of-flight (TOF), amplitude modulated continuous wave (AMCW), frequency modulated continuous wave (FMCW), etc.] of the LADAR. The theoretical analysis applies to all detection methods, since the range errors occur due to a significant drop in received signal amplitude. In Section 5, the theoretical model is analyzed to determine the parameters which cause the range errors.

The sensors used here are common models used in mobile robotics research, namely models from Riegl.[19] Experimental results are shown in Section 6 which demonstrate that such spurious range points can be reliably detected, provided the signal amplitude and orientation of the scanning optics are monitored with each range data value.

2. 3D SCANNING LADAR SYSTEMS

In this section, the LADAR scanning systems used in this work are introduced. The main LADAR is based on a 1D Riegl LD90-3300EHS-FLP model, as shown in Figure 1(a). This LADAR is a time-of-flight (TOF) based measurement system,[20] with a reported maximum range measurement capability of 400 m. The data acquisition rate of the sensor can be configured between a *single shot mode* of 12 kHz, to an *averaging mode* of 2 Hz, in which several samples are averaged before being output from the device.[1] The accuracy of the LADAR will be quantified in Section 3.3.

Figure 1. (a) 1D Riegl LADAR LD90-3300EHS-FLP model, (b) in-house developed 3D scanning mechanism, and (c) 3D Riegl LADAR LMS-Z210i. The 3D mechanism in (b) and the 3D LADAR in (c) allow continuous rotation of the scanning mirror about the vertical axis and simultaneous control of the mirror's elevation about a horizontal axis.

For robot navigation, a desirable feature of any ranging system is that it provides full 360° coverage around the robot in bearing, so that all objects of interest, within the field of view of the sensor can be "seen" from any vehicle orientation. Surprisingly, to the knowledge of the authors, few such affordable systems exist, possibly due to the difficulty in powering and controlling the elevation of the scanning mirror, while allowing continuous rotation in bearing.[21] Figure 1(b) shows a 3D scanning system developed at Nanyang Technological University (NTU) for this purpose.[22]

The scanning LADAR is to be used on board an outdoor terrain vehicle, which can traverse fields, hills and small trenches. As a consequence, the complete system can undergo significant changes in its roll and pitch angles as the vehicle moves. To take full advantage of the axis of elevation, twin axis rate gyros are used to create a quasigimbaled scanning system.[22] The aim of this system is to monitor the rate gyros and estimate the roll and pitch of the system, so that the elevation angle of the scanning mirror can be controlled as a function of its bearing angle. This is done to ensure that, as far as possible, the LADAR scans in the same plane (thus allowing the same potential objects to be sensed) as before any changes in

Figure 2. Received signal amplitude image recorded in a laboratory environment. Each pixel value is proportional to the received signal amplitude. The small circle (labelled "A") shows a zero-signal amplitude point.

Figure 3. The corresponding range image of the scan in Figure 2. Each pixel value is proportional to the estimated range. Darker pixels show closer objects.

the vehicle's roll and pitch angles occurred. The associated problems of gyro drift are discussed in ref. 22.

The 3D LADAR shown in Figure 1(c) is a LMS-Z210i model from Riegl.[19] Its rather slow rotating rate (at the highest rate of rotating, it takes around 20 s for the LADAR to fulfill a single 2D scan) limits its use in mobile robotic applications. However, in this work, this kind of 3D LADAR is still used for comparison with the LADAR of Figure 1(a) housed within the scanning mechanism in Figure 1(b).

3. RANGE ESTIMATION ERRORS IN LADARS

In order to place this work into perspective, an overview of three dominant kinds of range errors in a LADAR will be presented in this section, along with examples of how these errors affect range data scans. These three range errors can be split into systematic errors such as those caused by occlusion and cross-talk and random errors caused by noise.

3.1. Range errors due to occlusion

Figure 2 shows an intensity image [received signal amplitude. In the paper, the two words "intensity" and "signal amplitude" or "amplitude" will be used interchangeably. The intensity is a ratio, which is a dimensionless quantity that ranges from 0 (least reflective) to 255 (most reflective) which is based on the strength of the returned signal.] recorded from the 3D scanning Riegl LADAR [Figure 1(c)] in a laboratory environment. Each pixel row corresponds to a 330° section sweep of the environment. (This angle can be configured and for the LADAR's designing constraint, it can provide a 360° complete sweep only at a low rate of rotating.) Between each row of pixels, the elevation of the scanning mirror is changed by 0.4°. Figure 3 shows the corresponding range image where each pixel intensity value is proportional to range (darker pixels correspond to closer objects). Such images contain extremely useful information for robot navigation and offer the fundamental advantage over vision systems, in that range information is directly available.

In Figure 2, the small blue circle is shown to denote zero, or extremely low received signal amplitude values. These can be seen more clearly in Figure 4(a) where the amplitude of the received signal is plotted versus the scanning mirror's bearing angle, at a constant angle of elevation. This is taken from the middle row of pixels (elevation angle=40°) (the elevation angle ranges from 0° to 80° and hence 40° corresponds to the case for this sensor to scan within a plane) of Figure 2. Figure 4(b) shows the corresponding range versus bearing angle. When the amplitude reaches zero (or extremely low values) it can be seen that false ranges (range estimate=0m) occur. To elaborate further from exactly which artifacts within the environment these false range values occur, Figure 5 shows the planar range scan (looking from above) of the middle row pixels (LADAR mirror elevation=40°) in Figure 3.

In Figure 5, the environment is labelled with capital letters to denote the range readings corresponding to real objects in Figure 2. At the edge formed by "F," the black container, and "E," the background chairs and computers; the range readings are zero. This could, of course easily be detected as being false if its value were always zero. In reality, LADARs such as those from Riegl,[19] Acuity Research[23] and Sick (LADARs commonly used in mobile robotics research)[24] respond in different ways to such range discontinuities. It will be proved in Section 4 that *all* scanning LADARs with separated transmitter and receiver configurations will suffer a minimum in received signal amplitude due to the disparity between the transmitter and receiver aperture *irrespective of the technique used to estimate range*. The resulting effect of this reduced signal amplitude

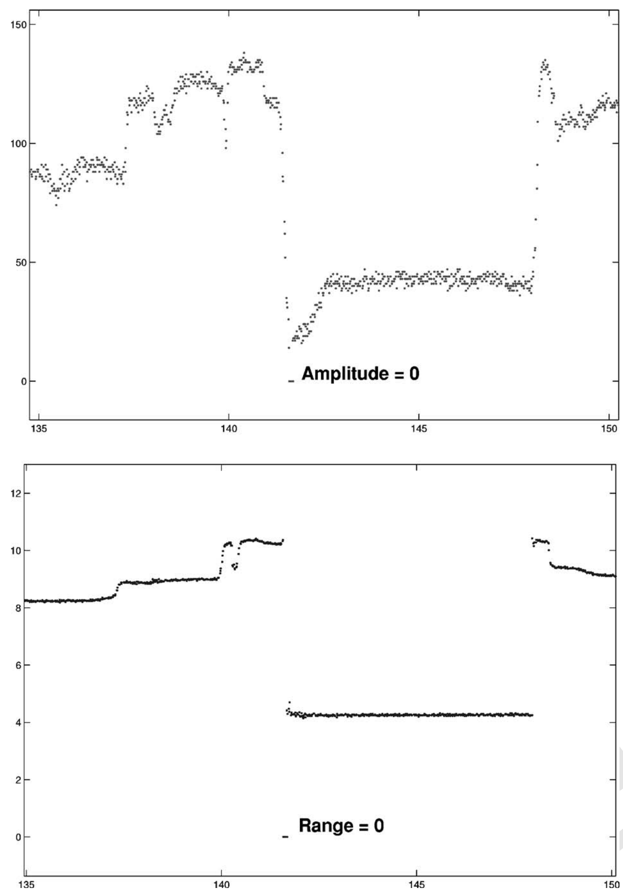

Figure 4. Received signal amplitude (a) and range (b) versus bearing corresponding to Figure 5. Plots are shown here with bearing ranging only from 135° to 150° to show the zero amplitude/range readings.

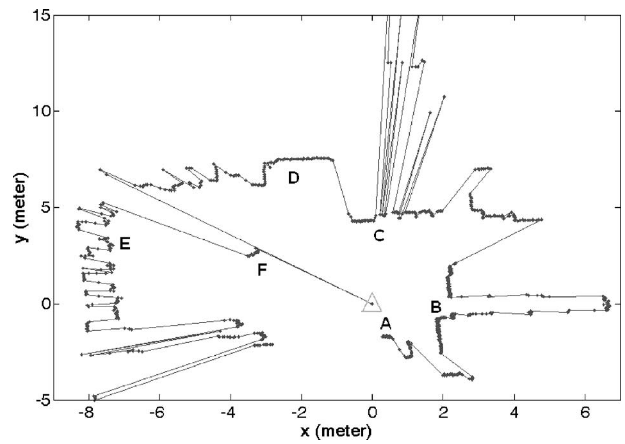

Figure 5. Plan view of the range data recorded at 40° angle of elevation. The small triangle shows the position of the LADAR system. In this environment each labelled object is, **A** a person in the right edge of Figure 2, **B** cubicles, **C** cabinets, **D** a door, **E** chairs and computers, and **F** a black container.

on the range estimate is then dependent on the measurement technique and is difficult to generalize to all LADARs. However, this paper will present a method to reliably predict such range failures based on other measurable quantities.

The effect of disparity or the "missing parts" problem in triangulation systems has of course been well documented,[12] however its subtle effect during the scanning of a LADAR and the resulting received amplitude profile does not appear to have been reported. This effect will be quantified in Section 4 and methods for the detection of such points will be presented in Section 6.

In the mobile robotics literature, scanned LADARs are used in countless navigational experiments.[5,8] Very few articles however, address the causes and effects of range errors associated with these sensors, which can be subtle and yet have a large impact on feature detection and data association algorithms. Notable exceptions are papers by Nitzan,[14] Hebert and Krotkov,[11] Reina and Gonzalez,[25] and more recent articles by Cang and Borenstein.[15] These articles address the issues of range errors caused by *random receiver/reflection noise*, *cross-talk* and *multiple path reflections*. For completeness, these effects are briefly analyzed for the LADARs used here, in the remainder of this section, after which Section 4 will focus purely on the fundamental problem of occlusion.

3.2. Range errors due to cross-talk effects

If the LADAR was perfect, range measurements would be independent of the reflective properties of the observed object. However, this is not true in reality. Radiation is absorbed by the reflecting surfaces, in some cases even to the point that the reflected signal is too weak to be detected correctly. Range errors of this type result in the estimated range being a function of the received signal amplitude. The extent of this effect depends on the detection electronics. In general, the receiver electronics function optimally only within a small dynamic range of received signal intensities in comparison with the large dynamic range of intensities which can be observed by the sensor. Therefore, materials which produce signals beyond the functioning dynamic range of the sensor can produce erroneous

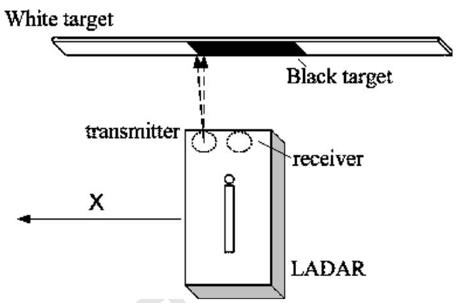

Figure 6. The LADAR is displaced past the edges formed by a black canvas target and a white target behind it.

range estimates. When the laser beam is projected at edges, the cross-talk effect becomes more noticeable.[11] Figure 6 shows an experiment to demonstrate this effect.

In Figure 6, the distance between the two canvas targets was zero. To position the 1D LADAR in Figure 1(a) precisely and to slide it in a controlled manner in a direction parallel to the target surfaces, it was mounted on the stacker of a milling machine and was translated to scan the discontinuities shown in Figure 6. The amplitude and range information were recorded and for one experiment are shown in Figure 7 to demonstrate the cross-talk effect. At the discontinuities formed by the two targets, range errors occur. The range errors (two "peaks") are of the order of several centimeters, much smaller compared to the range errors caused by the occlusion effect, which is several meters as shown in Section 3.1. However, the range errors caused by this cross-talk effect are "unpredictable,"[11] but can be related

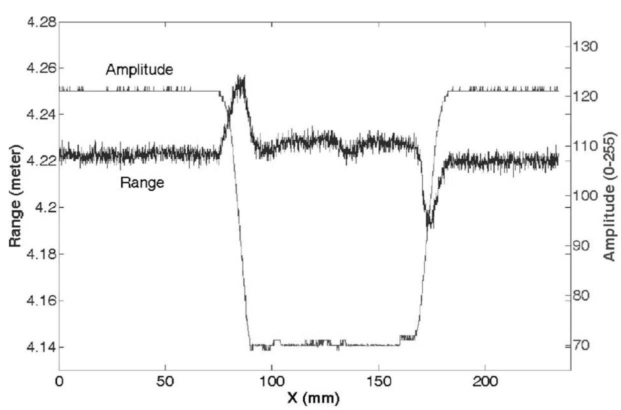

Figure 7. Mean range and amplitude for black and white targets to quantify the cross-talk effect.

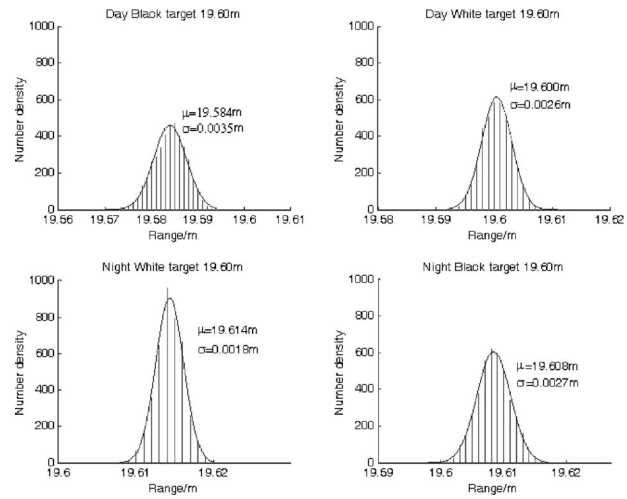

Figure 8. Range distributions showing the resulting range variance for varying target reflectivities and day/night conditions. In each case 4000 independent range readings were recorded from a fixed target.

to electronic interference within the LADARs or optical leakage directly between the transmitter and receiver.[1]

3.3. Random range errors

Most researchers model the range data from LADAR sensors as an estimated value with Gaussian noise.[8] In Figure 8, the histograms show the range data from the LADAR in Figure 1(a) at a constant target distance while the target reflectivity and illumination conditions were varied. The range data in each case approximately follows Gaussian distribution. Different target reflectivity and illumination conditions will affect the received signal amplitude according to Lambert's cosine law[1] and then the variance of the LADAR range data may also be affected. Hence, target reflectivity and illumination conditions with strong contrast, that is, black and white targets, day time and night time are chosen for this standard deviation test. However, it can be seen that for this LADAR, the range standard deviations are almost independent of these changing conditions and hence received signal strength. The range of the standard deviation is from 1.5 mm to 3.5 mm. That is to say, the random range errors are much smaller than the range errors caused by the occlusion effect and the cross-talk effect. This is true in many tested commercially available LADARs such as Riegl,[19] Sick,[24] and IBEO.[26]

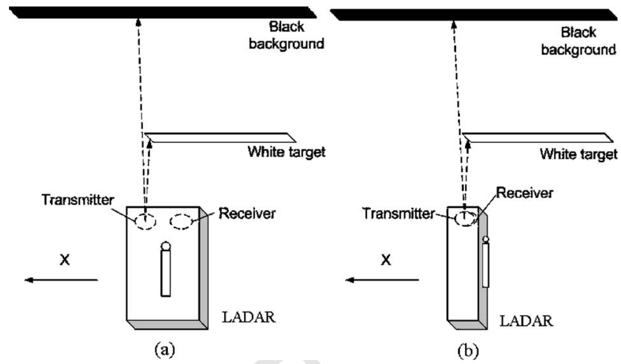

Figure 9. (a) The LADAR is displaced past an edge formed by a target and a background. (b) The sensor is rotated 90° so that the transmitter and the receiver are displaced in a "coaxial" manner relative to the vertical edge.

4. OCCLUSION DUE TO TRANSMITTER/RECEIVER SEPARATION

In order to predict what sensor and environmental parameters will cause range errors due to occlusion, the physics causing occlusion will be studied in this section and a theoretical model will be derived.

To study the occlusion effect, an experimental setup was made as shown in Figure 9. The 1D LADAR in Figure 1(a) was mounted on the stacker of a milling machine again and was translated to scan the edge of a target and its background as shown in Figure 9(a). The range and amplitude information during this process were recorded and for one particular experiment are shown in Figure 10. A minimum in the amplitude profile occurs because of the separated transmitter and receiver configuration of the sensor, as will be proved later in this section. There is a loss in received energy due to the noncoaxiality of the sensor. When the amplitude drops below the minimum working threshold of the LADAR, the range reading cannot be trusted (it often reads zero for the two LADARs in Figure 1 but in general it may read any arbitrary value and hence cannot be compensated by a simple low-pass filter). This is the occlusion effect.

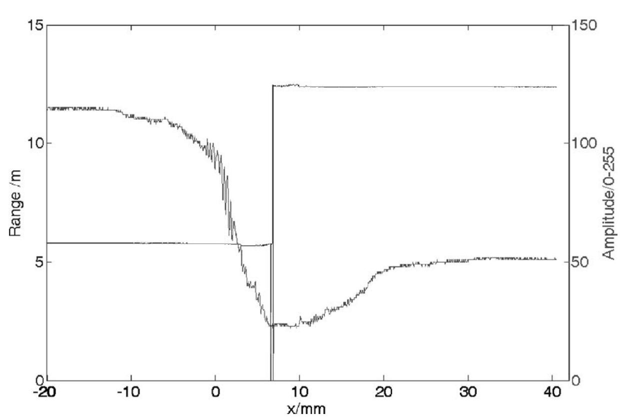

Figure 10. Range and amplitude when the 1D LADAR was displaced to scan the edge as shown in Figure 9(a).

Most LADAR sensors fall into two categories: coaxial and separated transmitter and receiver configurations. These configurations determine whether or not occlusion of reflected laser energy from targets occurs. The Riegl LADAR used in the analysis here has a separated transmitter and receiver configuration as shown in Figure 1(a). For the 3D Riegl LADAR as shown in Figure 1(c), the transceiver also has separated configuration.

The following analysis will mathematically derive the profile of the received signal power from noncoaxial LADARs, as their scanning mirrors rotate past a range discontinuity. It will then be shown how this profile can be used to predict when range errors, such as those shown in Figure 5 will occur, and how to detect them. In the analysis, the following assumptions are made:

1. The power in the transmitted and reflected light beams is uniformly distributed over the circular, cross-sectional area of the laser. (Note that the following analysis could be easily extended to other nonuniform optical power distributions.)
2. The received signal amplitudes from each individually illuminated target are known (i.e., they can be measured by the LADAR—P_1 and P_2).
3. Assumptions 1 and 2 allow that, without loss of generality, the scanning procedure can be modeled as with targets 1 and 2 parallel to the motion of the LADAR, irrespective of their true orientation. This is because the total received power is derived from the normal projections of the elliptical footprints, which are, of course, circular again, and independent of the orientation of the sensed target.
4. Due to assumption 3, the rotational, scanning motion of the LADAR's mirror Figure 1(b) can be modeled as a linear displacement of the LADAR's optical footprint past the edge. This assumption is valid, since, the true ro-

tational motion would simply make the targets relative orientation change slightly, relative to the LADAR, and since the normal projections of the elliptical footprints are considered, these orientations make no difference.

Initially, before the transmitted optical footprint intersects the edge, it will fully illuminate target 1 at range d_1, as shown in Figure 11(a). In this case, the received signal strength is P_1 watts, which can be measured if the amplitude of the received signal is available as in the case of the Riegl LADARs (and some Sick devices[24]). As the mirror scans, the projected optical foot print will eventually completely traverse the edge, so that it fully illuminates target 2 at range d_2. In this case it is assumed that the received signal strength is P_2 watts [Figure 12(b)].

In Figures 11(a) and 12(b), the received power *densities* of these *end conditions* are defined as

$$\mathcal{P}_{(x\leqslant 0)} = \frac{P_1}{\pi r_1^2} \quad \mathcal{P}_{(x\geqslant X_2)} = \frac{P_2}{\pi r_2^2} \tag{1}$$

where x is the motion of the LADAR measured from the edge of target 1 and r_1 and r_2 are the radii of the normal components of the optical footprints on targets 1 and 2, respectively. From Figures 11(a) and 12(b):

$$r_1 \approx \frac{d_1\alpha}{2} \quad r_2 \approx \frac{d_2\alpha}{2} \tag{2}$$

where α is the beam width of the transmitted laser.

The point $x=0$ is defined when the transmitted light beam just reaches the edge of target 1, as shown in Figure 11(a). The scanning of the LADAR's mirror is then considered to be equivalent to displacing the LADAR in the direction shown in Figures 11(a)–11(d) and Figures 12(a) and 12(b).

4.1. LADAR displacement $x\leqslant 0$ [Figure 11(a)]

The received signal power is given by

$$P_{(x\leqslant 0)} = \mathcal{P}_{(x\leqslant 0)}\pi r_1^2 = P_1 = \text{const} \tag{3}$$

Define X_1 as being the value of x at which target 2 just becomes visible to the receiver aperture. This scenario is depicted in Figure 11(c)

$$X_1 = \frac{(s-q)(d_2-d_1)}{d_2} \tag{4}$$

where s is the transmitter—receiver aperture separation and q is the effective radius of the receiver lens.

4.2. LADAR displacement $0\leqslant x< X_1$ [Figure 11(b)]

The received power in this interval is

$$P_{(0\leqslant x<X_1)} = \frac{A_1}{\pi r_1^2}P_1 \tag{5}$$

where it can be shown from Figure 11(b) that the illuminated area A_1 is

$$A_1 = r_1^2\left(\pi - \theta_1 + \frac{\sin 2\theta_1}{2}\right) \tag{6}$$

so that

$$P_{(0\leqslant x<X_1)} = P_1\left(1 - \frac{\theta_1}{\pi} + \frac{\sin 2\theta_1}{2\pi}\right)$$

$$\theta_1 = \cos^{-1}\left(1 - \frac{2x}{d_1\alpha}\right) \tag{7}$$

Equations (7) define the received power amplitude profile, which is expected when traversing the edge for $0\leqslant x< X_1$.

4.3. LADAR displacement $X_1\leqslant x<2r_1$ [Figure 11(d)]

The power received in the displacement interval $X_1 \leqslant x<2r_1$ results from the *two* foot print sections shown in Figure 11(d)

$$P_{(X_1\leqslant x<2r_1)} = \frac{A_1}{\pi r_1^2}P_1 + \frac{A_2}{\pi r_2^2}P_2 \tag{8}$$

where it can be shown from Figure 11(d)

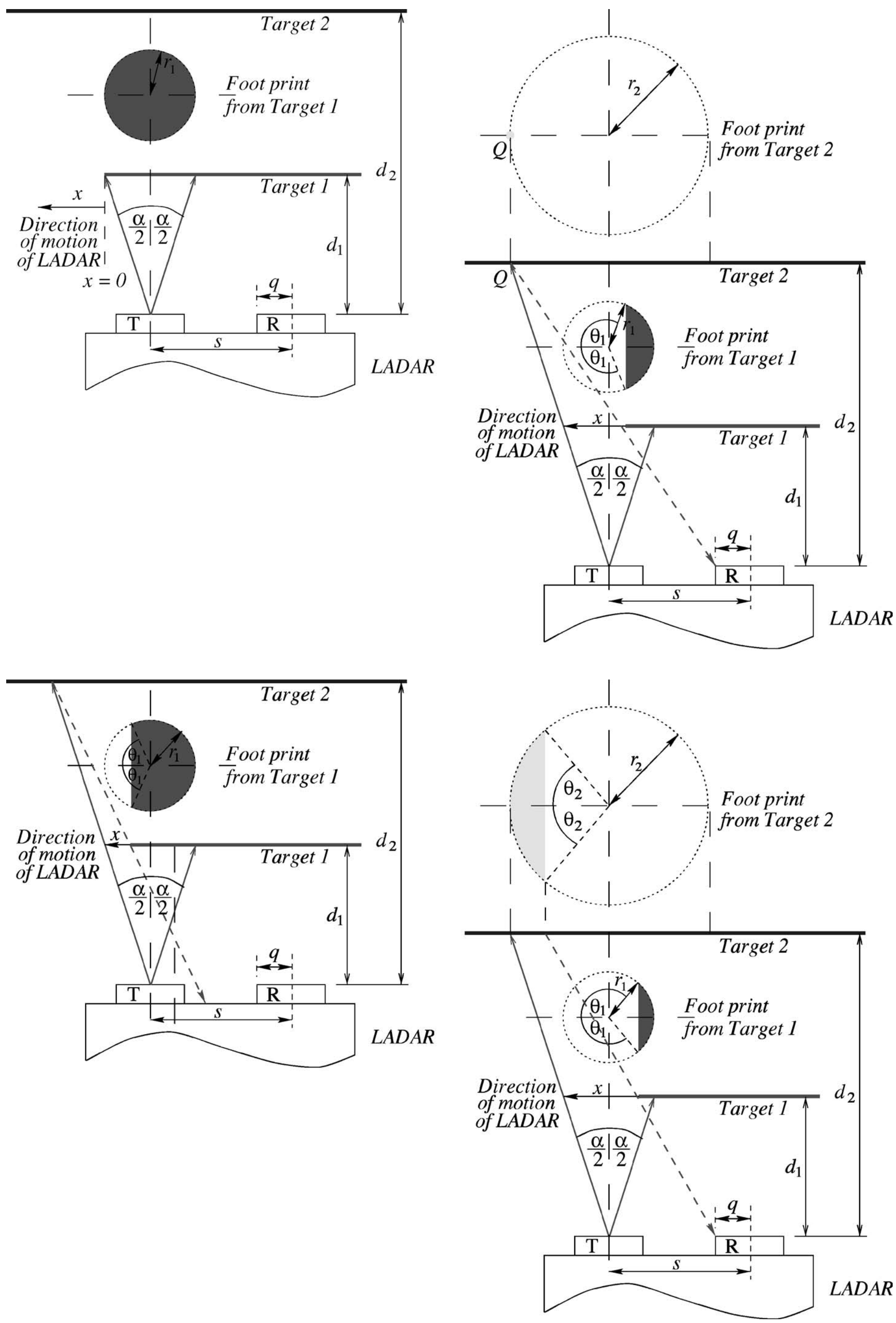

Figure 11. (a) Only target 1 is illuminated. (b) Target 2 is completely occluded due to the transmitter-receiver separation s. The footprint's area on target 1 is reduced. (c) Point Q on target 2 just enters the field of view of the receiver aperture. (d) Light now received from both targets 1 and 2.

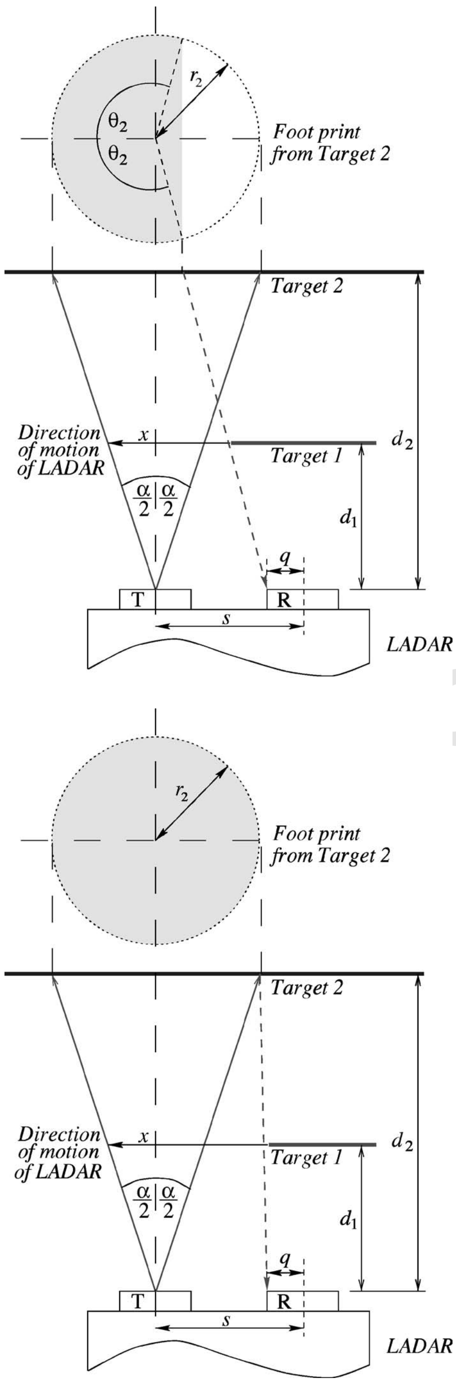

Figure 12. (a) Target 1 is no longer illuminated. Target 2 is partially occluded by target 1, due to transmitter-receiver separation s. (b) Light is now received from target 2 only, with no occlusion from target 1.

$$A_1 = r_1^2\left(\pi - \theta_1 + \frac{\sin 2\theta_1}{2}\right) \quad \theta_1 = \cos^{-1}\left(1 - \frac{2x}{d_1\alpha}\right) \tag{9}$$

as before, and

$$A_2 = r_2^2\left(\theta_2 - \frac{\sin 2\theta_2}{2}\right) \quad \theta_2 = \cos^{-1}\left[1 - \frac{2(x - X_1)}{d_2\alpha}\right] \tag{10}$$

so the received signal power in this interval is

$$P_{(X_1 \leqslant x < 2r_1)} = P_1\left(1 - \frac{\theta_1}{\pi} + \frac{\sin 2\theta_1}{2\pi}\right) + P_2\left(\frac{\theta_2}{\pi} - \frac{\sin 2\theta_2}{2\pi}\right) \tag{11}$$

Let $x = X_2$ be the displacement of the LADAR at which target 1 just fails to occlude target 2. In this case, geometrical considerations give

$$X_2 = \frac{(s - q)(d_2 - d_1)}{d_2} + d_1\alpha \tag{12}$$

4.4. LADAR displacement $2r_1 \leqslant x < X_2$ [Figure 12(a)]

The power received in the displacement interval $2r_1 \leqslant x < X_2$ results from the single foot print shown in Figure 12(a):

$$P_{(2r_1 \leqslant x < X_2)} = \frac{A_2}{\pi r_2^2} P_2 \tag{13}$$

where it can be shown from Figure 12(a):

$$A_2 = r_2^2\left(\theta_2 - \frac{\sin 2\theta_2}{2}\right) \quad \theta_2 = \cos^{-1}\left[1 - \frac{2(x - X_1)}{d_2\alpha}\right] \tag{14}$$

as before, so that the received signal power in this interval is

$$P_{(2r_1 \leqslant x < X_2)} = P_2\left(\frac{\theta_2}{\pi} - \frac{\sin 2\theta_2}{2\pi}\right)$$

$$\theta_2 = \cos^{-1}\left[1 - \frac{2(x - X_1)}{d_2\alpha}\right] \tag{15}$$

4.5. LADAR displacement $x \geqslant X_2$ [Figure 12(b)]

Finally target 2 is fully illuminated and the LADAR has been displaced enough, so that no part of the foot print is occluded from the LADAR's receiver aperture. In this case

$$P_{(x \geqslant X_2)} = p_{(x \geqslant X_2)}\pi r_2^2 = P_2 = \text{const} \tag{16}$$

Equations (3), (7), (11), (15), and (16) between them, when θ_1 and θ_2 are replaced by their respective functions of x, describe the complete expected received amplitude profile as the LADAR's transmitted laser is scanned past a range discontinuity. In Figure 13(a) (the red dotted profile), the amplitude profile is plotted versus the illuminated footprint displacement. Compared with the measured amplitude in Figure 10 [repeated in Figure 13(b) for comparison], the estimated profile in Figure 13(a) (the red dotted profile) is similar and the minimum value in the amplitude is almost the same. However the width of the change in the amplitude curve in the actual case (Figure 10) is slightly smaller than that in the simulated case [Figure 13(a), the red dotted profile]. The possible reason of the difference is due to the assumption that the laser energy is uniformly distributed over the beam cross section, which probably is not true. In reality, the laser energy concentrates around the center of the beam cross section, rather than being uniformly distributed, which causes the effective value of α, the beam width of the transmitted laser, to be smaller than the assumed value and then causes the effective foot print radii r_1 and r_2 to be smaller than the theoretical values [Eq. (2)]. Hence the actual LADAR displacement regions $X_1 \leqslant x < 2r_1$ and $2r_1 \leqslant x < X_2$ are smaller, which causes the width of the actual change in the amplitude curves to be smaller.

From Eqs. (3), (7), (11), (15), and (16), the complete expected received amplitude profile can be plotted versus LADAR beam displacement x. If the minimum value of the amplitude could be determined as a general function of the LADAR beam displacement x and the other factors (LADAR to target distances d_1 and d_2, received end condition powers P_1 and P_2, LADAR parameters s, q and α), then the precise conditions which cause this minimum to be below the minimum working amplitude of the LADAR could be examined. During LADAR design, the values of s, q and α could be selected which minimize the chances of the minimum amplitude being below this minimum detection threshold. During operation, recorded data from the LADAR (range/amplitude) could be used to reliably predict when the received amplitude will drop below the detection threshold.

The amplitude profile is divided into five segments by different ranges of x. Equations (3) and (16) show that the amplitude remains constant during the two segments $x \leqslant 0$ and $x \geqslant X_2$ respectively, and

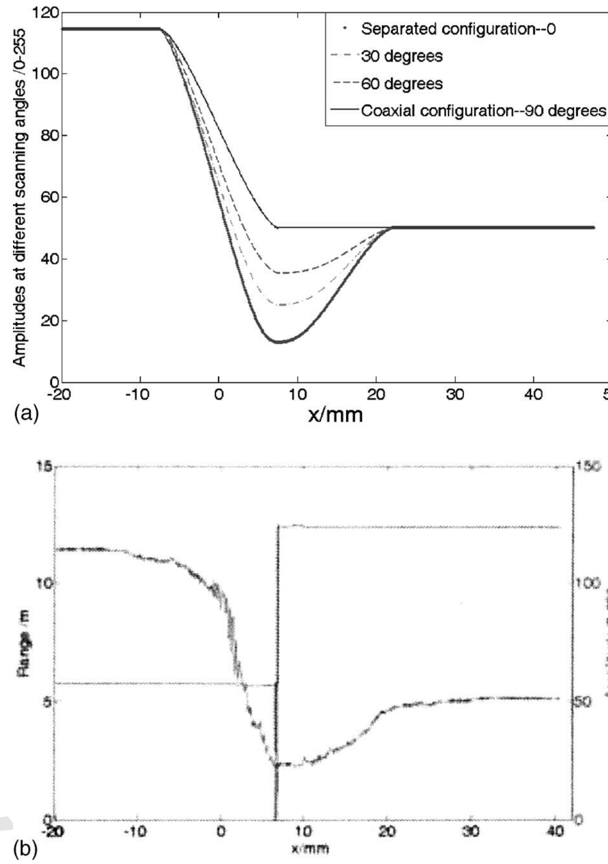

Figure 13. (a) Estimated amplitude profiles of separated transmitter and receiver configuration and "coaxial" configuration LADARs. In this case, the values of involving parameters are $d1=5.8$ m, $d2=12.6$ m, $P1=115$, $P2=50$, and $s-q=2.9$ cm. (b) Actual amplitude and range profiles corresponding to the red dotted one in (a).

the minimum amplitude cannot occur in these two segments. Analysis of the other three segments gives the following.

The first derivative of Eq. (7) with respect to x is

$$\frac{\partial p}{\partial x} = \frac{P_1}{\pi\sqrt{xd_1\alpha - x^2}}\left\{\cos\left[2\cos^{-1}\left(1 - \frac{2x}{d_1\alpha}\right)\right] - 1\right\} \leqslant 0,$$

$$0 \leqslant x < X_1 \tag{17}$$

$\partial p/\partial x$ is negative when $x < X_1$ so that the amplitude profile p is monotonously decreasing.

The first derivative of Eq. (15) is

$$\frac{\partial p}{\partial x} = \frac{P_2}{\pi\sqrt{(x - X_1)d_2\alpha - (x - X_1)^2}} \times\left\{1 - \cos\left[2\cos^{-1}\left(1 - \frac{2(x - X_1)}{d_2\alpha}\right)\right]\right\} \geqslant 0,$$

$$2r_1 \leqslant x < X_2 \tag{18}$$

When $2r_1 \leqslant x < X_2$, the first derivative of the amplitude profile p is positive, which means it monotonously increases. Hence, the minimum amplitude due to the discontinuity can only occur in the range $X-1 \leqslant x < 2r_1$. The simulated amplitude profiles in Figure 13(a) show that a minimum amplitude occurs if there is any separation between the transmitter and receiver. Differentiating Equation (11) and setting it to 0 would give the value at which the minimum amplitude occurs. Derivative of Eq. (11) is

$$\frac{\partial p}{\partial x} = \frac{P_1}{\pi\sqrt{xd_1\alpha - x^2}}\left\{\cos\left[2\cos^{-1}\left(1 - \frac{2x}{d_1\alpha}\right)\right] - 1\right\} + \frac{P_2}{\pi\sqrt{(x - X_1)d_2\alpha - (x - X_1)^2}} \times\left\{1 - \cos\left[2\cos^{-1}\left(1 - \frac{2(x - X_1)}{d_2\alpha}\right)\right]\right\} = 0,$$

$$X - 1 \leqslant x < 2r_1 \tag{19}$$

Equation (19) is however difficult to solve.

In Figure 13(a), individual estimated amplitude profiles corresponding to a certain transceiver separation angle of the LADAR relative to the sensed target are shown for particular values of $d1$, $d2$, $P1$, $P2$, α and $s-q$. In this paper, the transceiver separation angle θ is defined as the angle between the direction of the transmitted laser beam and the center line of the transceiver of the LADAR when the LADAR's scanning mirror rotates. In Figure 15(a), the transceiver separation angle 0° corresponds to the separated transceiver configuration, equivalent to the experimental set up of Figure 9(a) while in Figure 15(c) the transceiver separation angle is 90°, corresponding to the "coaxial" ("coaxial" only in the sense of scanning past *vertical* edges) type configuration equivalent to the set up in Figure 9(b). Figure 15(b) shows the general case with transceiver separation angle θ. As the transceiver separation angle increases, the minimum value of the amplitude profiles increases which means potential elimination of the measurement error at a certain angle. If the transceiver separation angle reaches 90° [as in Figure 9(b)], the transceiver configuration effectively becomes "coaxial" and the minimum in the amplitude profile disappears [as shown in Figure 13(a), the blue solid profile]. This is shown in Figure 14, which is the experimental result by using the setup in Figure 9(b). In Figure 14, it can be seen that the minimum in amplitude no longer exists as it was recorded with θ=90° [Figure 15(c)]. Note that the amplitude curve in this real case resembles the simulated one in Figure 13(a) (the blue solid profile, when θ=90°). Also note that after the range readings jump from the front target to the background, there is an overshoot which can cause an error up to around 10 cm. This overshoot error is probably due to the

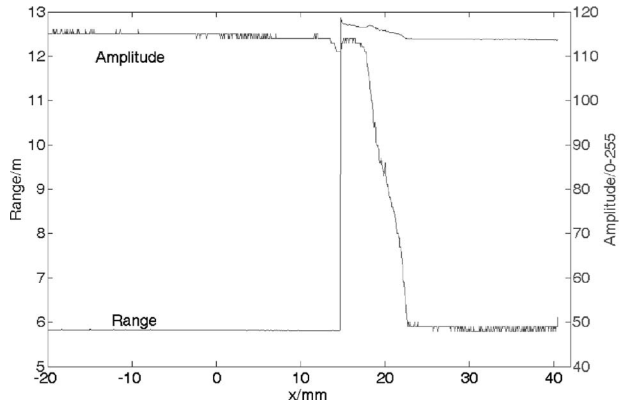

Figure 14. Range and amplitude when the LADAR was translated past the same vertical edge in Figure 9(a) in a "coaxial" manner.

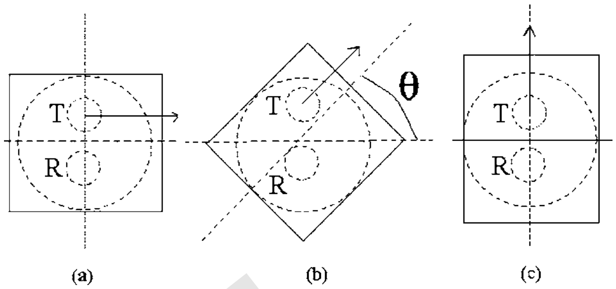

Figure 15. Top view of the scanning mirror in Figure 1(b). "T,R" denote the LADAR's transmitter and receiver and the red arrows denote the direction of transmitted laser beam. (a) $\theta=0°$, (c) $\theta=90°$, and (b) general case.

response of the LADAR electronics when suffering an abrupt range jump.

The above analysis was carried out with the 3D LADAR scanner in Figure 1(b). For the 3D LADAR in Figure 1(c), the rotating mirror rotates in unison with the transceiver and their relative position is constant. That means, for this kind of LADAR scanner, the transceiver is always "separated" [as the configuration in Figure 15(a)] no matter what the LADAR scanning mirror's real bearing angle is. When this LADAR scans past a vertical edge as in Figure 9, the estimated profile will always have the form of the red dotted curve in Figure 13. As shown in Figure 16, for this 3D LADAR, since the transceiver separation angle θ is effectively always 0°, it corresponds to the separated transmitter/receiver configuration in the 1D case.

5. CAUSES OF RANGE ERRORS—APPLYING THE "OCCLUSION" MODEL

The theoretical model derived in the previous section [Eqs. (3), (7), (11), (15), and (16)] can be used to estimate the received signal amplitude profile and hence predict and detect the range errors caused by this occlusion effect. However, it is more important for LADAR users or designers to know how to predict the range errors in real applications or possibly how to derive the necessary LADAR parameters in advance so as to avoid or minimize the chances of such errors. To avoid range errors the minimum amplitude in the profile must be increased to a value above the minimum detectable amplitude of the sensor itself. A solution to this problem is, of course, by decreasing the minimum detectable amplitude of the sensor. (This is, of course, already an optimization criterion for most LADAR manufactures.) In this section, the theoretical model will be analyzed to determine the effect of different LADAR design parameters and environmental parameters which can cause the received amplitude to fall below a predefined minimum value.

For LADARs of the type shown in Figure 1(b) or equivalently Figure 15, the fundamental parameter is the transceiver separation angle θ of the LADAR. For the 3D LADAR in Figure 1(c) or equivalently Figure 16, it is not affected by this parameter at all since the transceiver is always "separated" with respect to a vertical edge. In Figure 13, by rotating the scanning mirror of the LADAR from 0° to 90° equivalent to turning the mirror from the case in Figure 15(a)–15(c), the minimum amplitude keeps increasing.

In order to see what the amplitude profile will be at each transceiver separation angle, the estimated signal amplitude is shown versus the sliding distance (x in mm) and the transceiver separation angle (in degrees) in Figure 17, which corresponds to different transceiver configurations (varying θ in Figure 15) (the complete estimated amplitude profile is equivalent to setting the 1D sensor at a transceiver separation angle θ and allowing it to repeat the scan in Figure 9). The minimum detectable amplitude of this Riegl LADAR is assumed to be 18 (found by experiment), and as the transceiver separation angle θ reaches $(n+1/2)\pi$ rads (for integral values of n), there will be no minimum in the amplitude as the transceiver separation approaches the case of Figure 15(c) and then no range error will occur. In Figure 18, the minimum amplitude in each amplitude profile corresponding to a transceiver separation angle in Figure 17 is plotted versus the angle. Compared to the minimum detectable amplitude (the dotted line with amplitude=18), it can be seen that, the minimum will be larger than 18 and no range error will occur if $-160° \leqslant \theta \leqslant -20°$ and $20° \leqslant \theta \leqslant 160°$. Since the minimum detectable amplitude of each LADAR is different, the particular transceiver separation angular

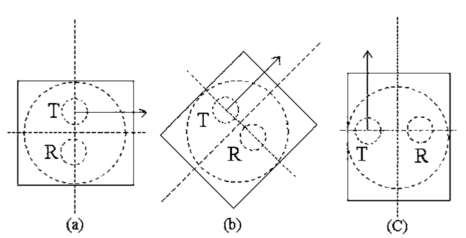

Figure 16. The scanning system of the Riegl LADAR LMS-Z210i [Figure 1(c)] is designed so as to maintain full separation between the transmitter and receiver with respect to vertical edges, at all mirror bearing angles.

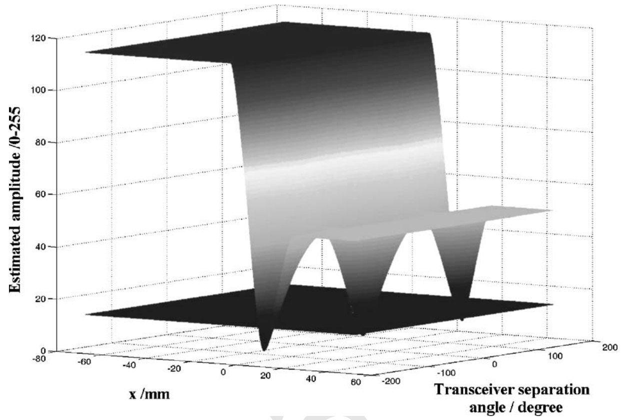

Figure 17. Signal amplitude versus the sliding distance x and the transceiver separation angle θ. The other parameters used were $d1=5.8$ m, $d2=12.6$ m, $P1=115$, $P2=50$, $s-q=2.9$ cm, and $\alpha=3$ mrad. The minimum detectable amplitude of the LADAR is plotted as the plane with amplitude=18.

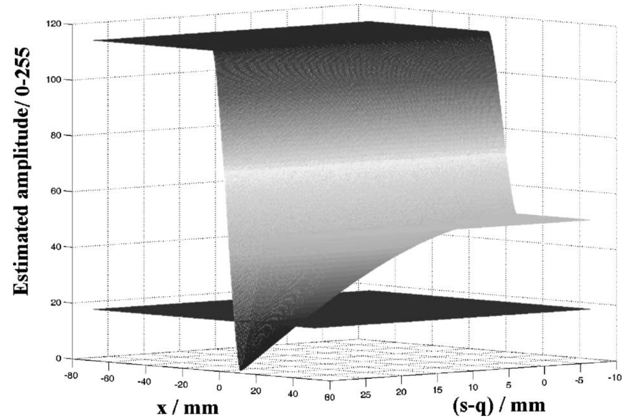

Figure 19. Estimated signal amplitude versus the sliding distance x and the transceiver separation $s-q$. The minimum detectable amplitude of the LADAR is plotted as the plane with amplitude=18.

range in which the range error will disappear depends on this value for the given device. For LADARs which maintain a constant separation between the transmitter and receiver [Figure 1(c)], the range errors can always occur.

The second parameter to be analyzed is a sensor parameter, the transceiver separation, $s-q$ in Eq. (4) with s being the transmitter—receiver aperture separation and q the effective radius of the receiver lens. As expected (see Figure 19), by decreasing $s-q$, the minimum amplitude value is also increased, thus decreasing the chances of false range values. During LADAR design, this parameter should be kept as small as possible while keeping the transmitter and receiver still separated to guarantee that all of the transmitted light leaves the LADAR.

Further parameters which affect the minimum value of the received amplitude are environmental ones, namely the distances and the reflectivities of the targets which form the scanned edge. In Figure 20, it

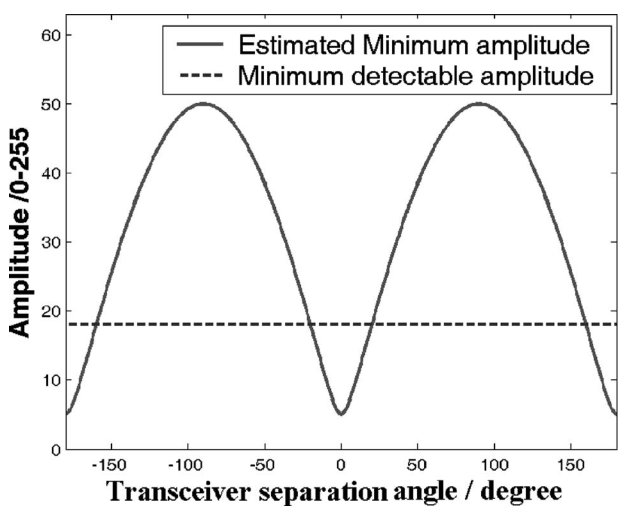

Figure 18. Minimum amplitude versus the transceiver separation angle θ. The minimum detectable amplitude of the LADAR is plotted as the line with amplitude=18.

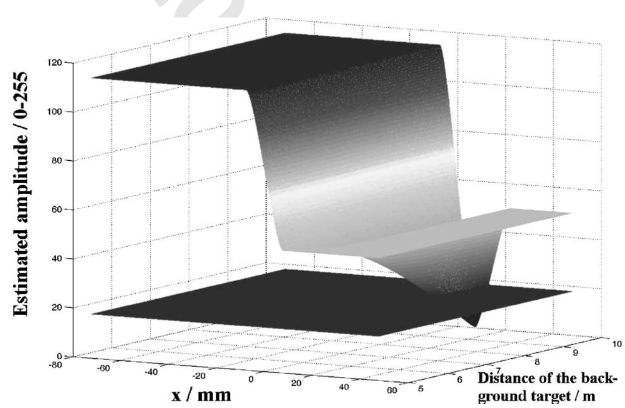

Figure 20. Estimated signal amplitude versus the sliding distance x and the distance of the background target $d2$. The minimum detectable amplitude of the LADAR is plotted as the plane with amplitude=18.

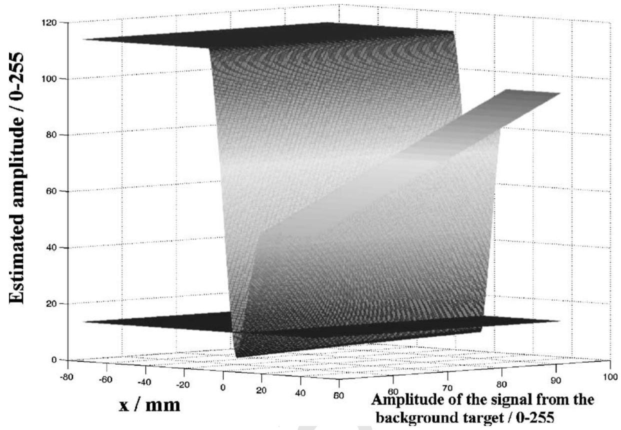

Figure 21. Simulated signal amplitude versus the sliding distance x and the amplitude of the signal from the background target. The minimum detectable amplitude of the LADAR is plotted as the plane with amplitude=18.

can be seen that if the distance of the background target is decreased so that the two targets are closer to each other, the minimum amplitude value is also increased. This makes sense since if the two targets are put at the same distance, the front target cannot occlude the reflected light from the background target.

In Figure 21, the received power P_2 from the background target is increased (corresponding to a higher reflectivity of that target), the minimum amplitude value is then also increased. *It is interesting to note, that the minimum in the amplitude profile is hardly affected by the power which is received by any one of the surfaces either side of the edge, when fully illuminated, i.e., the reflectivity of each individual surface*. For almost all combinations of edge separation $d_2 - d_1$, increasing the reflectivity of any one of the surfaces does not significantly increase the minimum in amplitude.

6. EXPERIMENTAL RESULTS

Finally, some experimental results are presented to show the effect of these different parameters on the

Figure 22. An intensity image of an semi-outdoors environment from a 3D LADAR. "A" in the figure denotes a container.

Figure 23. The corresponding range image of the scan in Figure 22. Darker pixels are closer to the sensor.

minimum amplitude and the occurrence of range errors. It will also be demonstrated how range errors can be avoided by selecting various parameters. First, a semistructured, outdoors environment (a car park area within the NTU campus) is used to show how to predict and detect the range errors due to this occlusion effect in LADAR scans by using the model derived in Section 4. Figures 22 and 23 show received amplitude and range images respectively recorded from the 3D LADAR scanner in Figure 1(b) in this environment. It can be seen from the right side of Figure 22 that there was a black container (positioned at "A") in front of a white wall. The container and the wall form an edge where the occlusion effect could possibly occur in a LADAR scan. The distances of the container and the wall to the LADAR's position were recorded and so were the received signal amplitudes. With this information, as shown in Figure 24, an amplitude profile (the red amplitude profile denoted as "Estimated amplitude" in the legend) similar to those in Figure 13 by using the theoretical model was pro-

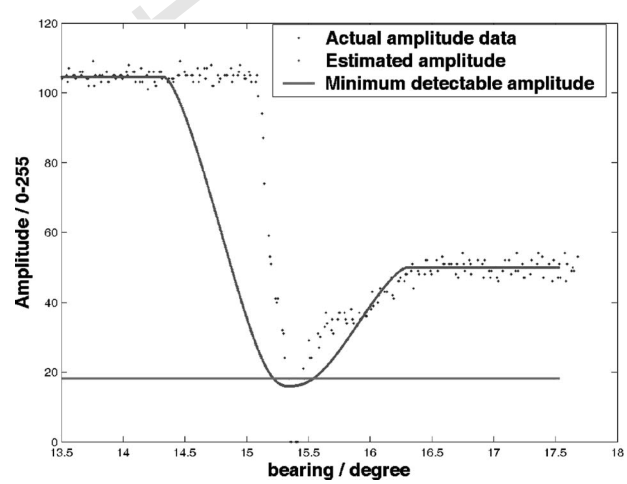

Figure 24. Estimated amplitude profile from the middle row (elevation angle is 40°) of the scan in Figure 22 compared with the actual amplitude profile.

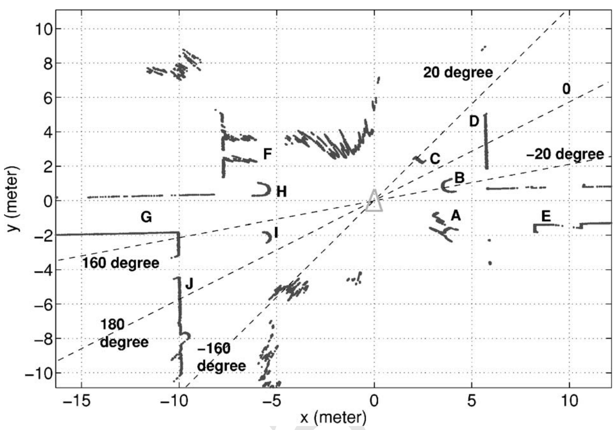

Figure 25. Plan view of the range data from the middle row (elevation angle is 40°) of Figure 22. The small blue triangle denotes the position of the LADAR. The red lines are range data. Capital letters A to J denotes objects in the environment, in which A denotes a person, B, H, I are pillars, C is a container, D is a background wall, F denotes bicycles, E, G represents a corridor, and J is another wall. The blue lines marked −20°, 0°, etc. are transceiver separation angle bounds defining areas where occlusion may occur (see Figure 18).

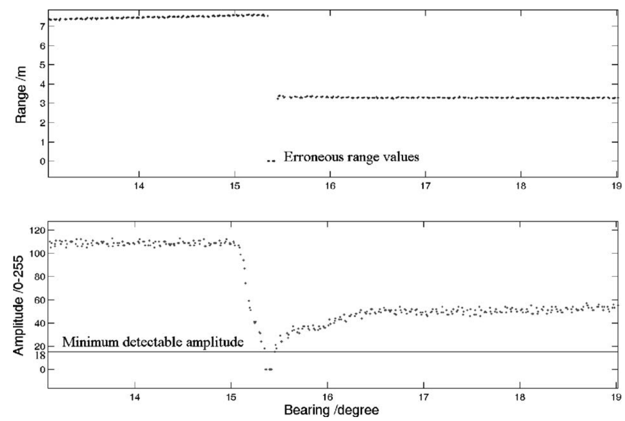

Figure 26. Range data and the signal amplitude data versus bearing from the same row (elevation angle 40°) of Figure 25.

duced. It can be seen that the minimum expected amplitude value in this case is lower than the LADAR's minimum detectable amplitude. Hence, in this case, range errors are expected at the edge. Compared with the actual amplitude data (the blue dotted profile) in Figure 24, it can be seen that the shape and minimum of the amplitude in both actual and estimated profiles are almost the same except that the width of the change in the estimated amplitude is larger than that in the actual one. The probable reason for this is that the effective laser beam width is smaller than the theoretical one used in the estimation since its energy is more concentrated at the center of the beam, as mentioned earlier.

Figure 25 shows the plan view of the range data from the middle row (elevation angle 40°) of Figure 22. According to Figure 18, false range values may occur at certain transceiver separation angle ranges, which are $-180° < \theta < -160°$, $-20° < \theta < 20°$, and $160° < \theta < 180°$, etc. and these regions are marked on Figure 25. The edge formed by the container and the wall falls in the transceiver separation angle range $-20° < \theta < 20°$ and then false range values are expected. Figure 26 shows the signal amplitude and the range data from the same row versus the LADAR mirror's transceiver separation angle to depict the false range values for the edge $C-D$ in Figure 25. It can be seen that at the edge, a minimum in amplitude occurs and its value is below 18, the minimum detectable amplitude of the LADAR, producing false range estimates as expected. At this point, the range value should be replaced with its prediction (if this is available as is the case in certain edge detection filtering algorithms such as ref. 3) if the range data is to be used in feature detection methods.[3]

Another experiment was carried out in an indoor environment to show how to predict the range errors caused by occlusion by using the theoretical model and how to avoid the errors by changing the environmental parameters according to the model. Figure 27 shows an intensity image recorded by the 3D LADAR in Figure 1(c) in the same laboratory as the one in Figure 2 and Figure 28 shows the corresponding range image.

In the environment, a black container (denoted "A" in the intensity image) formed an edge with the white door behind it. Again, the distances of the container and the door to the LADAR's position were measured and so were the amplitudes of signals from

Figure 27. Received signal amplitude image recorded in the same laboratory environment as that in Figure 2. "A" in the figure denotes a container.

Figure 28. The corresponding range image of the scan in Figure 27.

the two targets by the LADAR. With this information, an amplitude profile similar to those in Figure 13(a) by using the theoretical model was produced, as shown in Figure 29 (estimated amplitude profile 1). From this profile it can be predicted that the minimum amplitude value in this case is lower than the LADAR's minimum detectable amplitude and hence range error is predicted to appear.

Figure 30 shows the actual range and amplitude data versus the bearing angle of the LADAR from the same row as the estimated one. It can be seen that at the edge, the actual amplitude is below the minimum detectable one and an erroneous range point occurs in the range profile.

From the analysis in Section 5, four parameters (the transceiver separation angle θ, the transceiver separation $s-q$, the distances and the reflectivity of

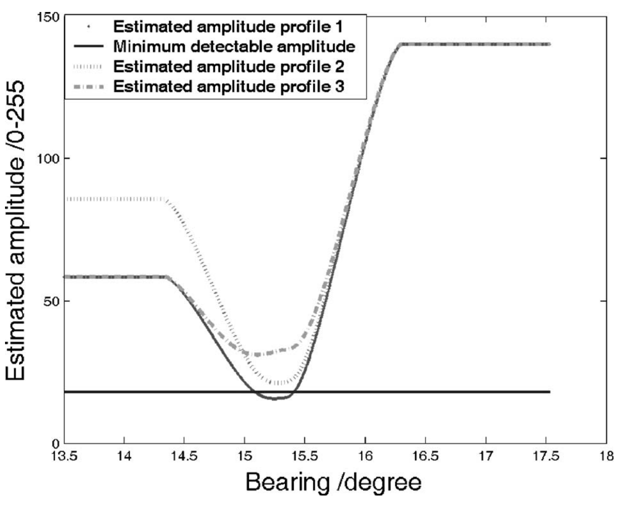

Figure 29. Estimated amplitude profiles: Estimated amplitude profile 1 corresponding to the middle row (elevation angle is 40°) of Figure 27; estimated amplitude profile 2 corresponding to the case of changing the black container in Figure 27 to white; estimated amplitude profile 3 corresponding to the case of enlarging the distance of the black container in Figure 27.

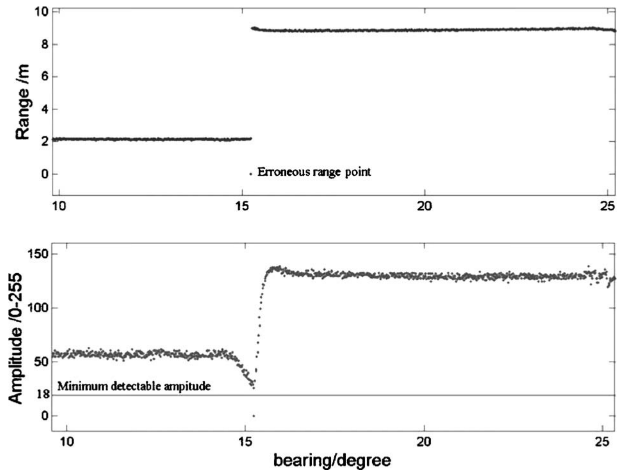

Figure 30. The actual range and amplitude data versus the bearing angle correspond to the estimated amplitude profile 1 in Figure 29.

the targets which form the scanned vertical edge) affect the minimum amplitude value at an edge. For this 3D LADAR [Figure 1(c)], the transceiver separation $s-q$ cannot be changed. Hence, here the environmental parameters–the reflectivity and distance of the target were changed to investigate the effects on occlusion. First, the black container was covered by a white canvas so as to increase its reflectivity. From the analysis used to produce Figure 21, the minimum amplitude should only slightly increase when increasing the reflectivity of either surface. By changing the amplitude information only, the theoretical model was used to estimate the amplitude profile again and it is shown in Figure 29 (estimated amplitude profile 2). In this profile, although the amplitude from the front target is greatly increased, the minimum amplitude increases only by a small amount, but remains above the minimum detectable value of the sensor, and hence the range error should be avoided. Figure 31 shows the actual range and amplitude data versus the bearing angle of the LADAR corresponding to the estimated profile 2 in Figure 29. It can be seen that the amplitude of the front target (the container) is increased and at the edge, the actual amplitude value is slightly above the minimum detectable one and no erroneous range points occur.

The white canvas cover was then removed and the distance of the black container was set to a larger value so that the distance between it and the white door behind it was reduced. By using this information, the amplitude profile was estimated again and shown in Figure 29 (estimated amplitude profile 3).

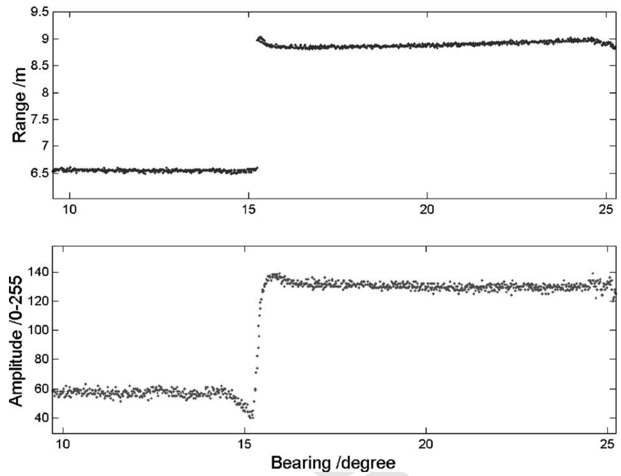

Figure 31. Actual range and amplitude data versus bearing angle corresponding to the estimated amplitude profile 2 in Figure 29.

From the estimated profile, it is seen that the minimum amplitude is increased and much larger than the minimum detectable value of the LADAR. Figure 32 shows the corresponding actual range and amplitude data versus the bearing angle when the range to the front target is increased. As expected, range errors are then avoided.

From the above analysis and results, it can be seen that the theoretical model is effective in predicting range errors caused by occlusion. After the range errors are detected, it is necessary to replace these erroneous points with their predictions when the LADAR is used in feature/range detection applications.[2,3]

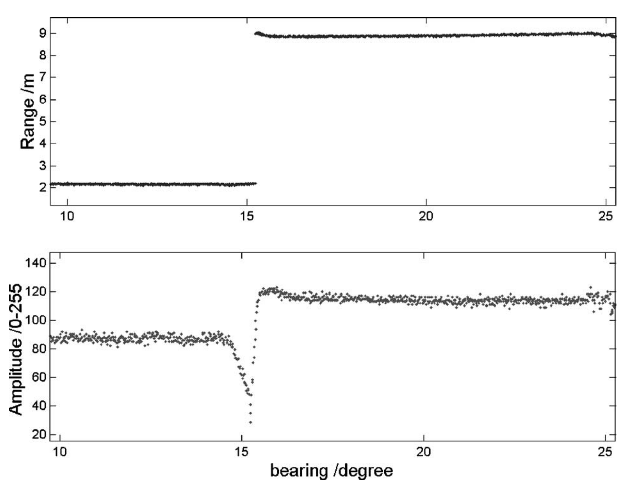

Figure 32. Actual range and amplitude data versus bearing angle corresponding to the estimated amplitude profile 3 in Figure 29.

7. CONCLUSIONS

This paper evaluates false range readings caused by occlusion effects when using LADARs having noncoaxial transmitter-receiver configurations. It has been shown that these range errors can be significantly larger than those caused by cross-talk effects and random noise. It has been shown analytically and experimentally that partial occlusion of the received laser light can occur in these LADARs when scanning edges (discontinuities) between neighboring targets at different ranges. A minimum in the received signal power will occur, which can be below the minimum operating signal power necessary for correct operation and hence cause erroneous range readings. For applications such as feature detection and data association, this effect will introduce unwanted measurement errors and can cause the failure of feature detection algorithms and range noise reduction techniques. However, by using the proposed received signal power model, such erroneous range values can be predicted, detected and removed before further processing.

Also, from this model, it can be seen that the minimum received signal power depends on sensor parameters such as the transmitter-receiver aperture separation and the transceiver separation angle, as well as environmental parameters such as the reflectivity and distance/separation of the targets. This dependency information is important for LADAR users as well as LADAR designers and allows them to avoid or, at least predict false range data caused by occlusion. This paper has shown that the chances of occlusion errors can be minimized by minimizing the separation of the LADAR's transmitter and receiver at the design stage. Further, it has been shown that a large separation of the targets being sensed is much more likely to cause false estimation than the reflective qualities of the targets themselves. Hence the derived models can be used to guarantee that all range values at edges will be sensed correctly within certain target separation bounds.

ACKNOWLEDGMENTS

This research was funded by the second author's AcRF Grant RG 10/01, Singapore. We would also like to thank Professor Wang Han, NTU for his help in providing various LADAR sensing equipment.

REFERENCES

1. M.D. Adams, Sensor modelling, design and data processing for autonomous navigation, World Scientific Publications, Singapore, 1999.
2. W.S. Wijesoma, K.R. S. Kodagoda, and A.P. Balasuriya, Road boundary detection and tracking using ladar, IEEE Transactions on Robots and Automation 20:(3) (2004), 456–464.
3. F. Tang, M. Adams, J. Ibanez-Guzman, and W.S. Wijesoma, Pose invariant robust feature extraction from range data with a modified scale approach, in Proc. of the IEEE International Conference on Robotics and Automation, New Orleans, USA, 2004.
4. K.S. Chong and L. Kleeman, Sonar feature based map building for a mobile robot, in Proc. of the IEEE International Conference on Robotics and Automation, Albuquerque, New Mexico, USA, 1997, pp. 1700–1705.
5. Jose Guivant, Eduardo Nebot, and Stephan Baiker, Autonomous navigation and map building using laser range sensors in outdoor applications, J. Rob. Syst. 17:(10) (2000).
6. S. Clark and G. Dissanayake, Simultaneous localisation and map building using millimetre wave radar to extract natural features, in Proc. of the IEEE International Conference on Robotics and Automation, Detroit, Michigan, USA, 1999, pp. 1316–1321.
7. C. Drocourt, L. Delahoche, E. Brassart, and C. Cauchois, Simultaneous localization and map building paradigm based on omnidirectional stereoscopic vision, in Proc. of the IEEE Workshop on Omnidirectional Vision (ICAR'01), Budapest, Hungary, 2001, pp. 73–79.
8. K.O. Arras, Feaute-based robot navigation in known and unknown environments (thesis no. 2765), Ph.D. dissertation, Swiss Federal Institute of Technology Lausanne, 2003.
9. M.D. Adams and P.J. Probert, The interpretation of phase and intensity data from AMCW light detection sensors for reliable ranging, Int. Journal of Robotics Research 15:(5) (1996).
10. R. Madhavan, H. Durrant-Whyte, and G. Dissanayake, Natural landmark-based autonomous navigation using curvature scale space, in Proc. of the IEEE International Conference on Robotics and Automation, Washington, DC, USA, 2002.
11. M. Hebert and E. Krotkov, 3-d measurements from imaging laser radars: How good are they? Image and Vision Computing 10:(3) (1992).
12. N. Pears and P. Probert, Active Triangulation Rangefinder Design for Mobile Robotics, in Proc. of the IEEE/RSJ International Conference on Intelligent Robots and Systems, Raleigh, NC, USA, 1992.
13. T. Einsele, Localization in indoor environments using a panoramic laser range finder, Ph.D. dissertation, TU München, Fakultät für Elektro- und Informationstechnik, 2002.
14. D. Nitzan, A.E. Brain, and R.O. Duda, The measurement and use of registered reflectance data in scene analysis, Proceedings of IEEE, 65, (1977), 206–220.
15. C. Ye and J. Borenstein, Characterization of a 2-d laser scanner for mobile robot obstacle negotiation, in Proc. of the IEEE International Conference on Robotics and Automation, Washington, DC, USA, 2002.
16. M.J. Brownlow, A time-of-fight optical range sensor for mobile robot navigation, Ph.D. dissertation, University of Oxford, UK, 1993.
17. J. Nieto, J. Guivant, E. Nebot, and S. Thrun, Real time data association for fastslam, in Proc. of the IEEE International Conference on Robotics and Automation, Taipei, Taiwan, 2003.
18. L. Perera, S. Wijesoma, and M. Adams, On multidimensional assignment data association for simultaneous robot localisation and mapping, in Proc. of the IEEE International Conference on Robotics and Automation, New Orleans, USA, 2004.
19. (2003) Riegl Optical Sensors. [Online]. Available: http://www.riegl.co.at
20. J. Borenstein, B. Everett, and L. Feng, Navigating Mobile Robots: Systems and Techniques, A. K. Peters, Ltd., Wellesley, MA, 1996.
21. O. Wulf, B. Wagner, K.O. Arras, and H.I. Christensen, 2d mapping of cluttered indoor environments by means of 3d perception, in Proc. of the IEEE International Conference on Robotics and Automation, New Orleans, USA, 2004.
22. L.M.P. Emily and L.S. Wai, Acquisition of scanned outdoor optical range data for robot navigation, Nanyang Technology University, Tech. Rep., 2003.
23. (2005) Laser Measurement Sensors Acuity. [Online]. Available: http://www.acuityresearch.com/
24. (2005) Sick. [Online]. Available: http://www.sick.com
25. A. Reina and J. Gonzalez, Characterization of a radial laser scanner for mobile robot navïgation, in Proc. of the IEEE/RSJ International Conference on Intelligent Robots and Systems, Grenoble, France, 1997.
26. (2005) IBEO. [Online]. Available: http://www.ibeo-as.de/